Hindawi
Journal of Nanomaterials
Volume 2022, Article ID 7373631, 11 pages
https://doi.org/10.1155/2022/7373631

Research Article

Effect of Joule Heating and Thermal Radiation of MHD Boundary Layer Oldroyd-B Nanofluid Flow with Heat Transfer over a Porous Stretching Sheet by Finite Element Method

Hakeem Ullah,[1] **Mehreen Fiza**,[1] **Kamal Khan**,[1] **Shamaila Batool**,[2] **S. M. Ghufran**,[1] **and Seham M. Al-Mekhlafi**[3]

[1]*Department of Mathematics, Abdul Wali Khan University, Mardan, Khyber Pakhtunkhwa, Pakistan 23200*
[2]*Institute of Numerical Sciences, Kohat University of Science and Technology, Kohat, Pakistan*
[3]*Department of Mathematics, Sana'a University, Yemen*

Correspondence should be addressed to Seham M. Al-Mekhlafi; smdk100@gmail.com

Received 11 January 2022; Revised 21 August 2022; Accepted 7 September 2022; Published 3 October 2022

Academic Editor: Taza Gul

In this study, an incompressible two-dimensional Oldroyd-B nanofluid steady flow past a stretching sheet considering the outcomes of magneto-hydrodynamics (MHD) and porous medium with magnetic, electrical, and thermal radiation effects is investigated. Using a similarity transformation, the governing equations in the form of partial differential equations (PDEs) are converted into a nonlinear ordinary differential equations (ODEs) system. The acquired system is numerically solved by the finite element method (FEM). The effects of physical parameters like Deborah numbers "β_1" and "β_2", Brownian motion "N_b", thermophoresis parameter "N_t", Prandtl parameter "Pr", Lewis number "L_e", thermal conductivity "k", dynamic viscosity "μ", magnetic and electric effects as "M" and "E_1", and thermal radiation effect "Rd" on the flow are studied in detail. For higher N_b values, regional Nusselt numbers are increasing in magnitude. The local Sherwood number's size rises for high N_b numbers.

1. Introduction

The fluid which obeys the Newton's law of viscosity is known as the Newtonian fluid, whereas the non-Newtonian fluid is recognized as to be the satisfaction of the Newton's law of viscosity [1, 2]. The non-Newtonian fluid dragged the attraction of the researchers due to its significant applications in industrial and engineering such as mud drilling, plastic polymers, optical fiber, metal cooling and wire of polymer plates, damping agent in braking devices, and protective devices [3–5]. Sakiadis introduced the concept of flow due to a stretching sheet [6]. Scientists used this concept to develop the new results to various fluids [7–19]. Magyar and Keller extended this concept by using it as the exponential stretching sheet [20]. The boundary layer flow (BLF) of an incompressible fluid over a stretching sheet and the viscoelastic fluids is used commonly in engineering and industrial developments. The field has attracted researchers in the last few decades. In industries, BLF is used like wrapping thermal, cooling plates, condensation of thin film, fiber glass, heat exchangers, plastic processing, cosmetics, geology composites, paint flow, adhesives, tower generators, accelerators, electrostatic filters, and droplet filters [3, 4, 5]. By immersing them in quiescent liquids, many metal processes need to cool continuously such as fibers. The BLF is used by many scientists. The BLF based on the exponential stretching is studied by Bidin and Nazar who study the BLF due to exponential stretching sheet with thermal radiations [21]. This experiment is further extended with the partial slip effect by Mukhopadhyay and Gorla [22]. Singh and Agarwal [23] study the thermal radiation effect of the boundary layer flow with exponential stretching. The BLF and heat transfer HT over a moving surface are studied by Tsou et al. and Elbashbeshy [24, 25]. Choi proposed the concept of nanofluid in 1995 [26]. The nanofluid has many industrial and engineering applications like heat exchangers, engine radiators, and cooling processes [27, 28]. Khan et al. [29, 30] investigated the BLF of a nanofluid in a porous material. The thermal effect of the nanofluid flow of the boundary layer on the moving surface in various conditions was presented by Olanrewaju et al. [31], Crane [7], Koo and Kleinstreuer [32], and Khan et al. [29, 33]. The porous material containing the pores and the skeletal portion of the material is known as a matrix. The pores are filled by a fluid under consideration. Fiza et al. studied the nanofluid flows in a porous medium with viscoelastic properties [34]. The recent development in the study of nanofluid by considering various physical effects can be seen in [29, 33–59]. From the literature survey, it is clear that the effect of Joule heating and thermal radiation of MHD boundary layer Oldroyd-B nanofluid flow with heat transfer over a porous stretching sheet is not studied. This article is aimed at studying the effect of Joule heating and thermal radiation of MHD boundary layer Oldroyd-B nanofluid flow with heat transfer over a porous stretching sheet by a numerical computation method known as finite element method (FEM). The basic fundamental equations Navier-Stokes equations and continuity are used for the mathematical formulations. After using the similarity transformation, the formulation in the form of PDEs is converted into ODEs. The FEM is used for the solution of the modeled problem [60–63]. The physical paramaters are discussed with the help of graphs and tables. Organisation of the paper is as follows: Section 1 is dedicated to introduction, Section 2 to problem formulation, Section 3 to solution techniques, Section 4 to results and discussions, and Section 5 to conclusions.

2. Problem Formulation [57]

Consider the nanofluid motion of an incompressible two-dimensional Oldroyd-B across a stretching sheet. Nanoparticles are saturated when the sheet is stretched at $y = 0$, and the flow is originated at $y > 0$. The fluid is electrically conducted in the existence of magnetic field $\vec{B} = (0, B_0, 0)$ and electric field $\vec{E} = (0, 0, -E_0)$ which follow the Ohm's law $\vec{J} = \sigma(\vec{E} + \vec{V} \times \vec{B})$. The sheet is stretched linearly $u(x) = ax$, where "$a > 0$" and the sheet is considered as porous. The sheet velocity is taken parallel to the flow. The inducted magnetic field and Hall current effects are disregarded due to the minute magnetic field. The governing equations are as follows:

$$
\begin{aligned}
&u_x + v_y = 0,\\
&uu_x + vv_y + A_1\left(u^2 u_{xx} + v^2 u_{yy} + 2uvu_{xy}\right)\\
&\quad = v\left(u_{yy} + A_2 uu_{xyy} + vu_{yyy} - u_x u_{yy} - u_y v_{yy}\right)\\
&\quad + \frac{\sigma}{\rho}\left(E_0 B_0 - B_0{}^2 u\right) - \frac{v}{k}u,\\
&uF_x + vF_y = \alpha\left(F_{xx} + F_{yy}\right) + \tau\left\{D_B\left(C_x F_x + C_y F_y\right)\right.\\
&\quad + \left(\frac{D_t}{F_\infty}\right)\left[\left(F_x\right)^2 + \left(F_y\right)^2\right] + \frac{\sigma}{\rho}\left(uB_0 - E_0\right)^2 - \frac{\partial q_r}{\partial y},\\
&uC_x + vC_y = D_B\left(C_{xx} + C_{yy}\right)\\
&\quad + \left(\frac{D_F}{F_\infty}\right)\left(F_{xx} + F_{yy}\right) \cdot D_B\left(C_{xx} + C_{yy}\right) + \left(\frac{D_F}{F_\infty}\right)\left(F_{xx} + F_{yy}\right).
\end{aligned}
\tag{1}
$$

Here u, v represent the velocity components, fluid density ρ, kinematic viscosity v, electrical conductivity σ, A_1/A_2 the relaxation/retardation parameters, the thermal diffusivity α, the temperature T, the concentration C, D_B the Brownian diffusions, D_T the thermophoretic diffusion coefficient, and $\tau = (\rho c)_p/(\rho c)_f$ the nanoparticle to fluid heat capacity. ρ_p represents ithe idensity iof iparticle, $\vec{J}$ is the Joule current, σ is the electrical conductivity, and $\vec{V}$ is the velocity field of the flow. iIf $Y \longrightarrow \infty$, then the values of F and C are, respectively, F_∞ and i C_∞ as shown in Figure 1.

q_r represents the radioactive heat fluctuation that is proposed by Rosseland approximation like as follows:

$$
q_r = -\frac{16\varphi}{3K}\frac{\partial T^4}{\partial y}, \tag{2}
$$

where K represents the mean absorption coefficient and φ denotes the Stefan Boltzmann constant. By Taylor series equation, we obtain the following:

$$
T^4 = T_0{}^4 + 4T_0{}^3\left(T - T_0\right)^2 + \cdots \tag{3}
$$

On ignoring higher-order terms, we have the following:

$$
T^4 = 4TT_0{}^3 - 3T_0{}^4. \tag{4}
$$

Inserting Equation (10) in Equation (8), it reduced to the form of the following:

$$
\frac{\partial q_r}{\partial y} = -\frac{16T_C^3\varphi}{3K}\frac{\partial^2 T}{\partial y^2}. \tag{5}
$$

The boundary conditions are as follows:

$$
\begin{aligned}
&u(x) = ax, v = 0, C = C_0, F = F_0, y \longrightarrow 0,\\
&u(\infty) = 0, v(\infty) = 0, C = C_\infty, F = F_\infty, y \longrightarrow \infty.
\end{aligned}
\tag{6}
$$

Using the similarity transformation,

$$
\begin{aligned}
\psi &= (av)^{1/2} x F(\eta),\\
\theta(\eta) &= \frac{F - F_\infty}{F_w - F_\infty},\\
\phi(\eta) &= \frac{C - C_\infty}{C_w - C_\infty},\\
\eta &= \sqrt{\frac{a}{v}}y.
\end{aligned}
\tag{7}
$$

Using the stream function as $u = \partial\psi/\partial y$ and $v = -\partial\psi/\partial x$, we get the following:

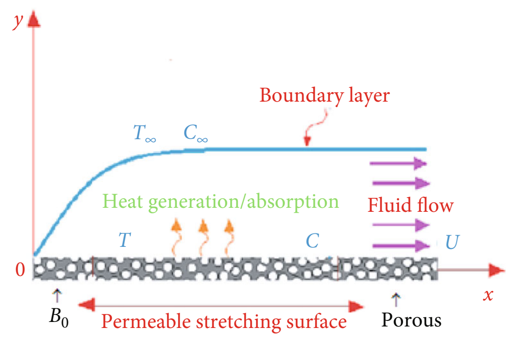

FIGURE 1: Schematic diagram of the flow.

$$f''' - f'^2 + ff'' + \beta_1\left(f^2 f''' - 2ff'f''\right) + \beta_2\left(ff'''' - \left(f''\right)^2\right) + M^2\left(E_1 - f'\right) - \kappa\left(f'\right) = 0, \tag{8}$$

$$\left(1 + \frac{4}{5}\mathrm{Rd}\right)\theta'' + \Pr\left(\theta\theta' + N_b\left(\theta'\phi'\right) + N_t\left(\theta'\right)^2\right) + M^2\Pr\left(f' - E_1\right)^2 = 0, \tag{9}$$

$$\phi'' + L_e\Pr\left(f\phi'\right) + \frac{N_t}{N_b}\theta'' = 0, \tag{10}$$

with

$$f(0) = 0, f'(0) = 1, f'(\infty) = 0,\ f''(\infty) = 0, \tag{11}$$

$$\theta(0) = 1,\ \theta(\infty) = 0, \tag{12}$$

$$\phi(0) = 1, \phi(\infty) = 0, \tag{13}$$

where $\beta_1 = aA_1, \beta_2 = aA_2$ are the Deborah numbers, $\Pr = \nu/\alpha$, is the Prandtl number, $N_b = (\rho c)_p D_B (C_w - C_\infty)/\nu(\rho c)_\rho$ and $N_t = (\rho c)_p D_T (T_w - T_\infty)/\nu(\rho c)_\rho$ are the Brownian and thermophoresis parameters, respectively, and $L_e = \alpha/D_B$ is the Lewis number.

Also,

$$\mathrm{Nu}_x = \frac{xq_w}{\alpha(T_w - T_\infty)}, \tag{14}$$

$$\mathrm{Sh}_x = \frac{xq_m}{D_B(C_w - C_\infty)}, \tag{15}$$

where $q_w = -\alpha(\partial T/\partial y)_{y=0}, q_m = -D_B(\partial C/\partial y)_{y=0}$ are the heat and mass flux, respectively.

The dimensionless form of Equation (14) is given as follows:

$$\mathrm{Re}_x^{-1/2}\mathrm{Nu}_x = -\theta'(0), \quad \mathrm{Re}_x^{-1/2}\mathrm{Sh}_x = -\phi'(0), \tag{16}$$

where $\mathrm{Re}_x = u_w(x)x/\nu$iis the Reynolds local, $\kappa = \nu/k$ is the porosity parameter, $M^2 = \sigma B_0^{\,2}/\rho a$ is the magnetic variable, and the electric parameter is $E_1 = E_0/B_0 ax$.

3. Finite Element Method

The FEM is a powerful method to evaluate the nonlinear differential equations and can be used to engineering problems such as fluid mechanics, biomathematics, physics, and channel process [49–51].

The important steps of FEM are as follows:

(1) Discretization into finite elements of the infinite domain

(2) Generation of component equations

(3) Gathering component equations

(4) Imposing boundary conditions

(5) Evaluation of gathered equations

Iterative approach can be applied in the last step.

A grid sophistication experiment is performed via dividing the domain in consecutive grids sized 81×81, 101×101 and 121×121 in z direction. Four functions are to be assessed at each node, and assembly of element equations, we get 404 nonlinear equations. An iterative scheme is acquired for solving the system introduced by BCs. If the relative difference among the sequential iteration is fewer than 10^{-6}, so the solution is considered as convergent. The code is run for various grid sizes and observed that the solution is free of the grid. The effect of the step size for step $h = 0.01$ is verified by achieving an excellent agreement for different profiles.

4. Results and Discussion

4.1. Figures Discussions. The nonlinear system of ODEs (Equations (8)–(13)) constrained by boundary conditions (Equations (11)–(13)) is assessed numerically by FEM. Figures 2–22 describe the actions of emerging parameters like Prandtl parameter Pr, relaxation time constant β_1, retardation time constant β_2, Brownian parameter N_b, Lewis number L_e, thermophoresis parameter N_t, and porosity parameter κ on velocity profile $f'(\eta)$, mass fraction function $\phi(\eta)$, and temperature profile $\theta(\eta)$. Figures 2–4 represent the effect of β_1 on $f'(\eta)$, $\theta(\eta)$, and $\phi(\eta)$. $\beta_1$which is a function of relaxation timeA_1assists the flow due to the viscoelastic characteristics of fluids. The BL thickness and the velocity profile $f'(\eta)$ increased by increasing the values of β_1. Also by the increase of β_1, both $\theta(\eta)$ and $\phi(\eta)$ of the mass fraction increase. The effects of β_2 on $f'(\eta)$, $\theta(\eta)$, and $\phi(\eta)$ are given in Figures 5–7. Since the retardation time of the fluid increases the fluid movement, so as a result, $f'(\eta)$, $\theta(\eta)$, and $\phi(\eta)$ increases by increasing β_2. The effect of the porosity number for the velocity profile is given in Figure 8. It is noticed that by increasing the porosity parameter, the velocity profile decreases. Since in the porous medium, there exist

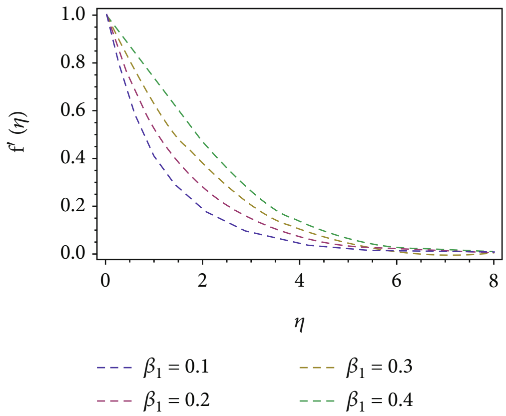

Figure 2: $f'(\eta)$ versus β_1.

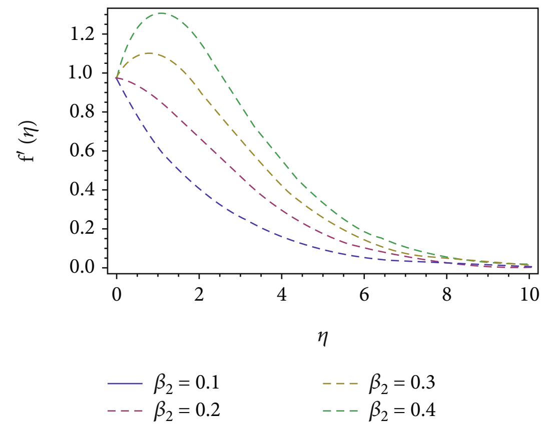

Figure 5: $f'(\eta)$ versus β_2.

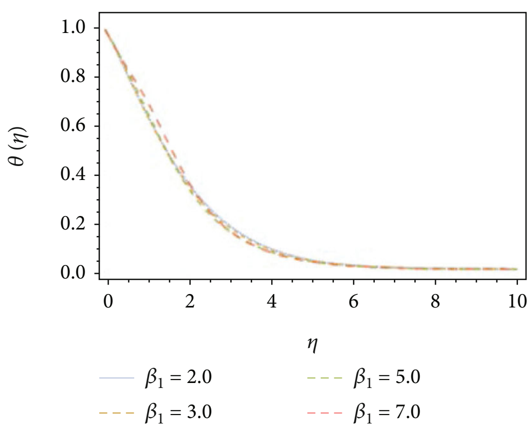

Figure 3: $\theta(\eta)$ versus β_1.

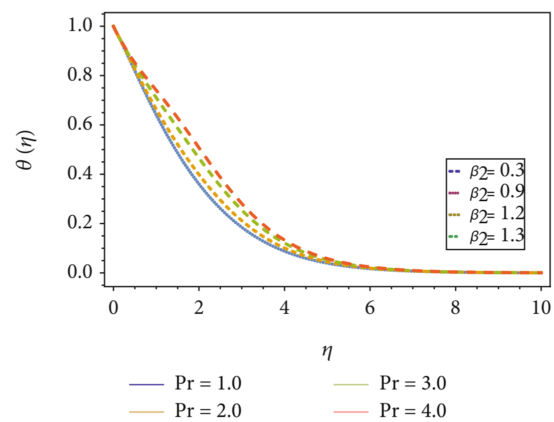

Figure 6: $\theta(\eta)$ versus β_2.

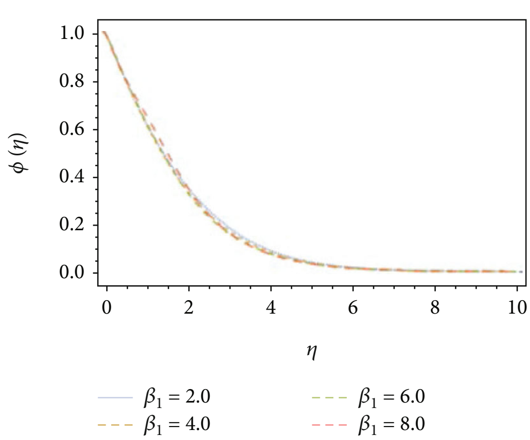

Figure 4: $\phi(\eta)$ versus β_1.

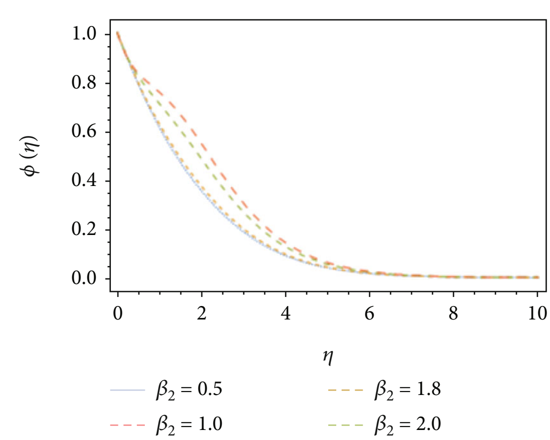

Figure 7: $\phi(\eta)$ versus β_2.

the porous holes and these holes reduce the velocity profile. The Lewis numbers are plotted for the temperature and concentrations profiles in Figures 9 and 10. An increase in the Lewis value caused to increase $\theta(\eta)$ and $\phi(\eta)$. The impacts on mass fraction function $\phi(\eta)$ of Brownian motion and temperature profile $\theta(\eta)$ and thermophoresis parameters are displayed in Figures 11, 12, 13, and 14, respectively. By increasing the values of N_b, the temperature profile increases while the concentration profile first decreases near the boundary and then increases as can be seen in Figures 11

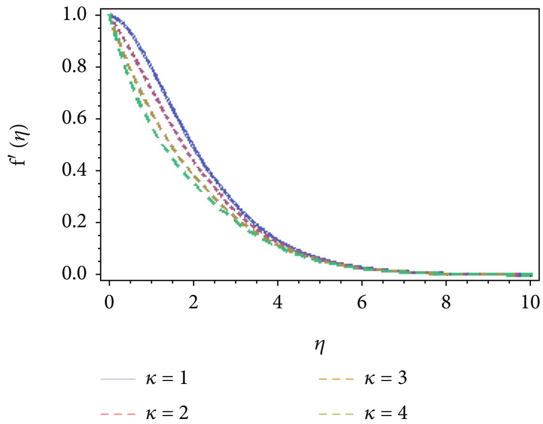

Figure 8: $f'(\eta)$ versus k.

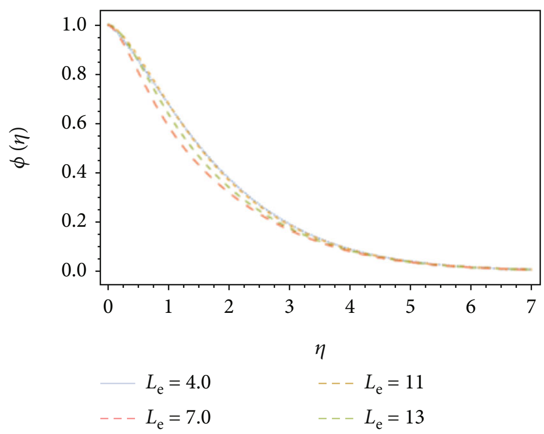

Figure 9: $\theta(\eta)$ versus L_e.

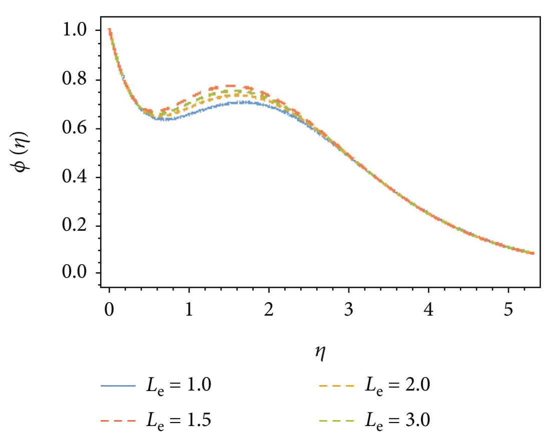

Figure 10: $\phi(\eta)$ versus L_e.

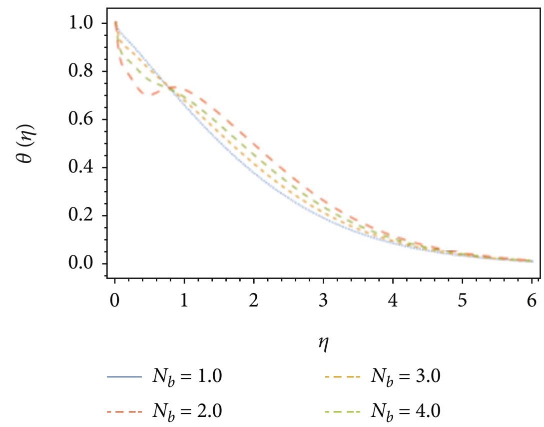

Figure 11: $f'(\eta)$ versus N_b.

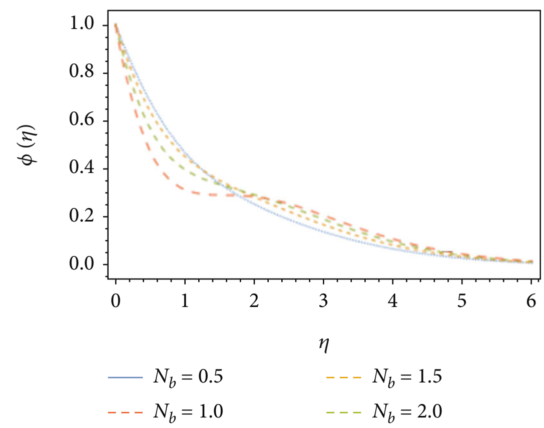

Figure 12: $\phi(\eta)$ versus N_b.

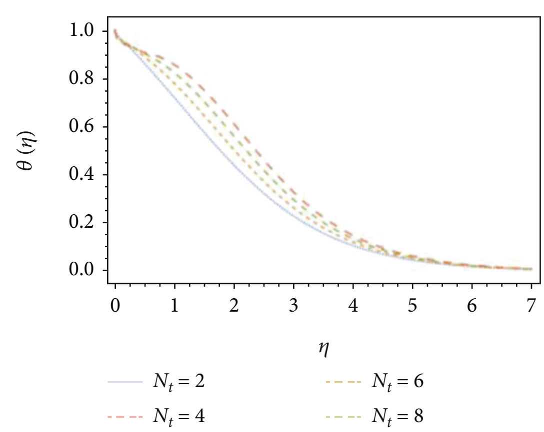

Figure 13: $\theta(\eta)$ versus N_t.

and 12; for the effect of N_t, it is noticed that by uplifting N_t, the temperature profile increases while the concentration profiles decrease can be seen in Figures 13 and 14. The effects of the Prandtl number on the temperature and concentration profiles are presented in Figures 15 and 16. Higher values of Prandtl numbers caused to decrease the temperature and concentration profiles. It is due to the fact that the Pr has an inverse relation with α, increasing Pr is basically to reduce the value of α which turn to reduce the elastic collision of the nanoparticles caused to reduce the

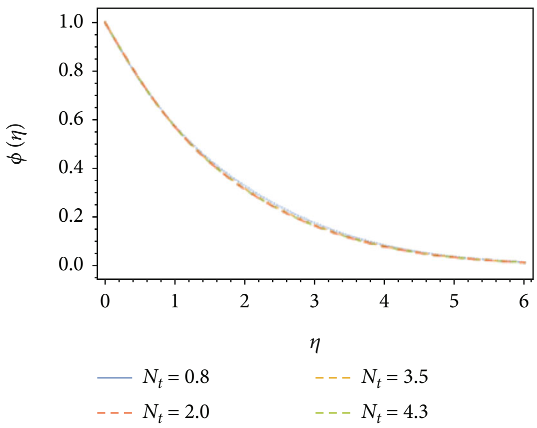

Figure 14: $\phi(\eta)$ versusN_t.

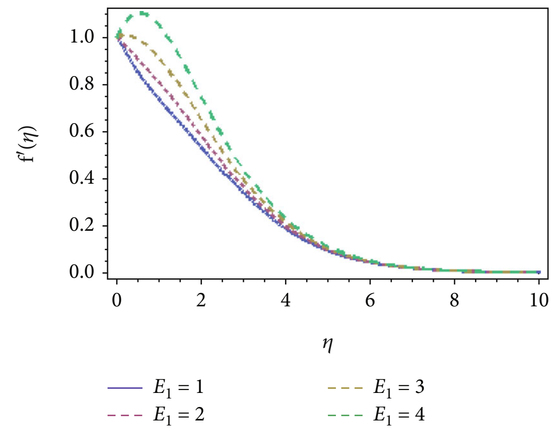

Figure 17: $f'(\eta)$ versus E_1.

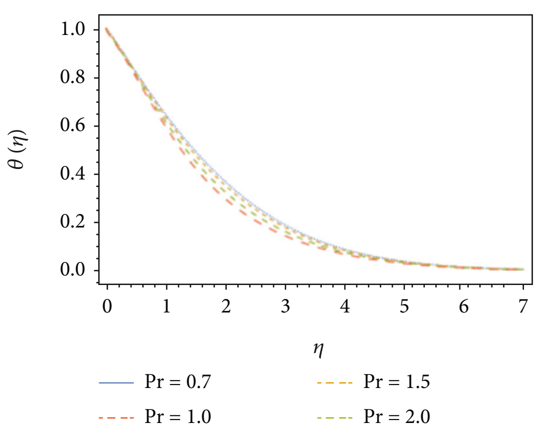

Figure 15: $\theta(\eta)$ versus Pr.

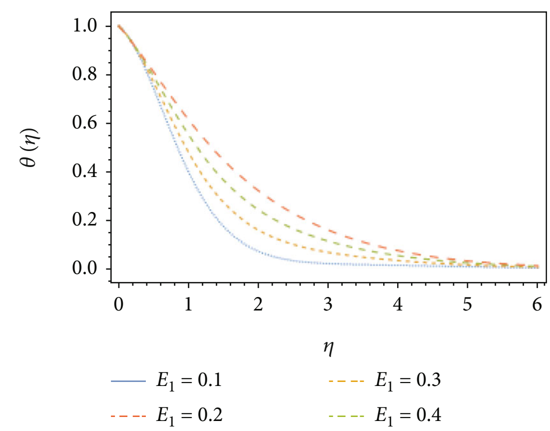

Figure 18: $\theta(\eta)$ versus E_1.

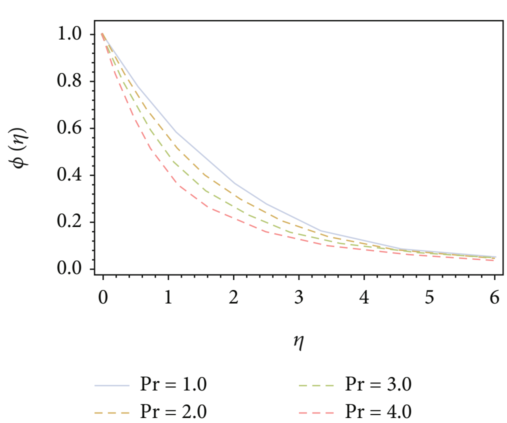

Figure 16: $\phi(\eta)$ versus Pr.

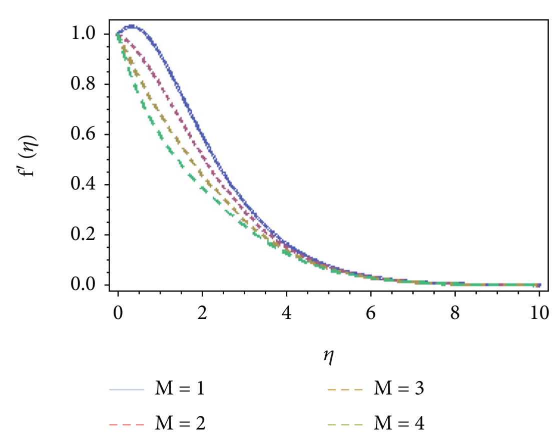

Figure 19: $f'(\eta)$ versus M.

profiles of concentration and temperature. The effects of the electric field E_1 on the velocity and temperature profiles are given in Figures 17 and 18, respectively. Increase in E_1 causes to increase the profiles of temperature and velocity. Also, the effects of the magnetic field on velocity and temperature profiles are given in Figures 19 and 20. Increase in magnetic field causes to decrease the velocity profile, whereas by increasing the magnetic field decreases the temperature profile. The magnetic field is put in perpendicular to the flow and it resisted the flow; thus, the velocity profile

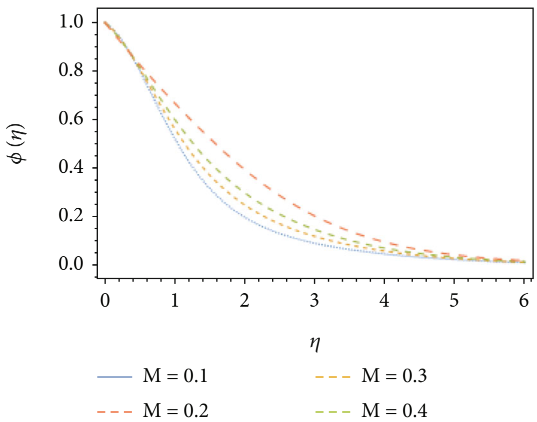

Figure 20: $\theta(\eta)$ versus M.

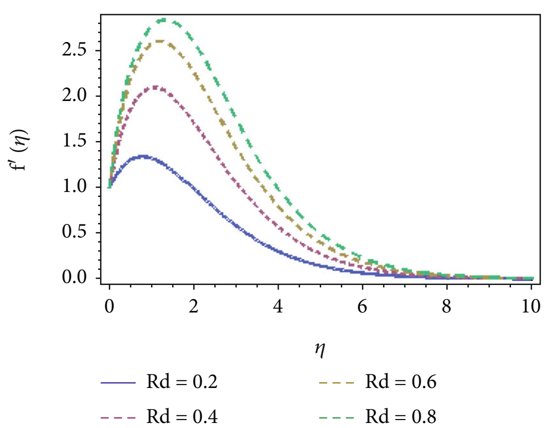

Figure 21: $f'(\eta)$ versus Rd.

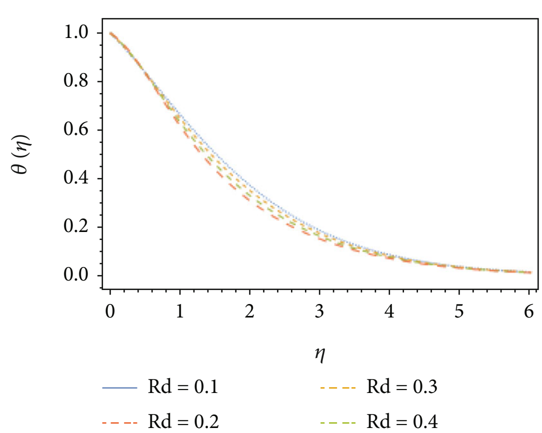

Figure 22: $\theta(\eta)$ versus Rd.

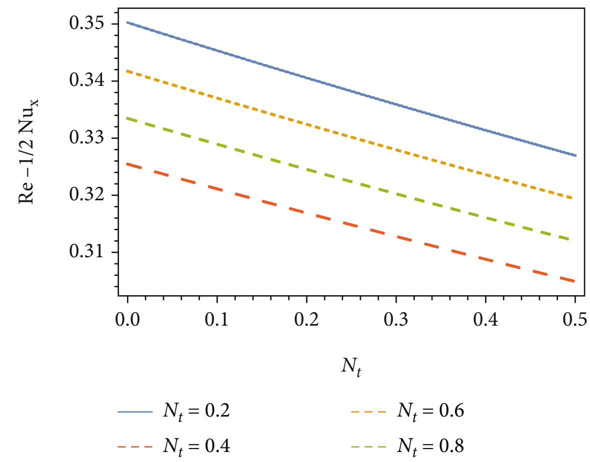

Figure 23: Nusselt number versus N_t.

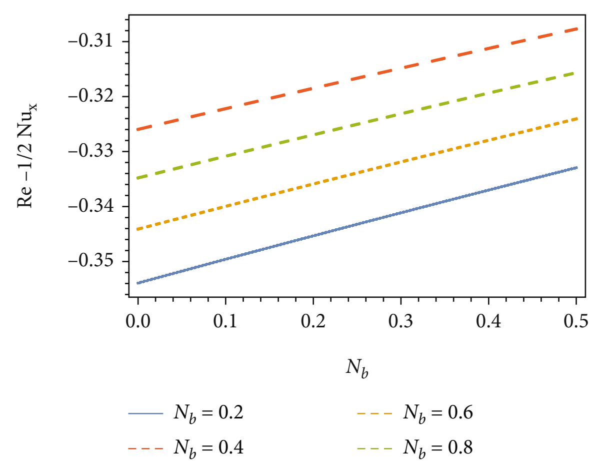

Figure 24: Nusselt number versus N_b.

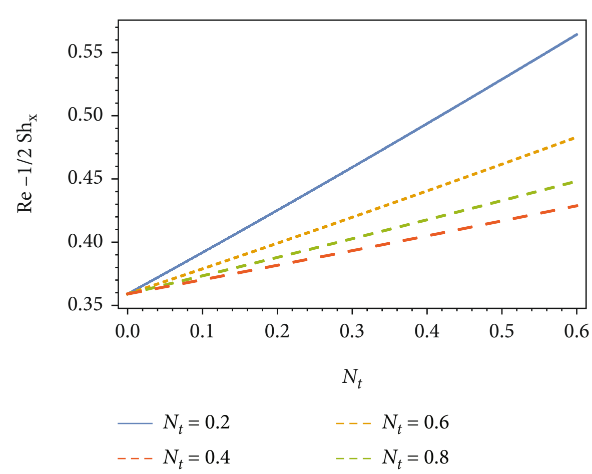

Figure 25: Sherwood number versus N_t.

reduced. The effect of the thermal radiations on the velocity and temperature field is given in Figures 21 and 22. Increase in thermal radiation caused to increase/decrease the velocity and temperature profiles. Results on the Sherwood number of the Brownian parameter, the Nusselt number, and thermophoresis parameter are given in Figures 23–26. It is noticed that the Nusselt number falls by rising N_t, whereas

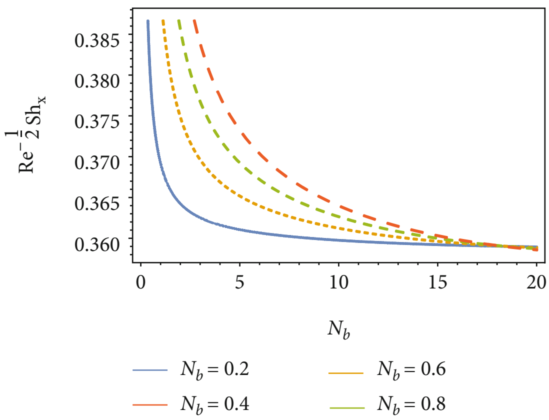

Figure 26: Sherwood number versus N_b.

Table 1: Numerical values of the local Nusselt number $Re^{-1/2}Nu_x$.

N_b/N_t	0.2	0.4	0.6	0.8
0.1	0.345332	0.337005	0.328932	0.321109
0.2	0.340533	0.332416	0.324528	0.316885
0.3	0.335903	0.327949	0.320241	0.312776
0.4	0.331372	0.323636	0.316071	0.308779
0.5	0.326962	0.319368	0.312013	0.304892

Table 2: Numerical values of the local Nusselt number $Re^{-1/2}Nu_x$.

N_t/N_b	0.2	0.4	0.6	0.8
0.1	-0.344720	-0.335351	-0.326466	-0.318049
0.2	-0.340555	-0.331372	-0.322668	-0.314424
0.3	-0.336454	-0.327456	-0.318931	-0.310857
0.4	-0.332416	-0.323620	-0.315252	-0.307347
0.5	-0.328441	-0.319805	-0.311629	-0.303894

Table 3: Numerical values of the Sherwood number $Re^{-1/2}Sh_x$.

N_b/N_t	0.2	0.4	0.6	0.8
0.1	0.555100	0.759519	0.970036	1.186100
0.2	0.457804	0.560222	0.665774	0.773986
0.3	0.425221	0.493763	0.564315	0.636564
0.4	0.408919	0.460513	0.513555	0.567815
0.5	0.399130	0.440547	0.483077	0.526535

the Nusselt number rises by rising N_b as given in Figures 23 and 24. The effects of N_t and N_b on the Sherwood number are given in Figures 25 and 26.

4.2. Tables Discussions. In Tables 1–4, an increase inN_t caused to reduce the Sherwood numbers and an increase in $N_b$caused to rise the Sherwood number. The Nusselt number decreases whenever the Pr is less than L_e and increases when the Pr is greater than L_e for N_b and N_t. However, the Sherwood number decreases with the rise of N_b and N_t for both the cases when the Pr is greater or less than L_e. Lastly, low thermal conductivity is caused by a high Prandtl fluid which decreases conductivity, resulting in an increase in sheet surface heat transfer. In the absence of non-Newtonian parameters β_1 and β_2, it is observed that the effect of both temperature and concentration profiles of nanoparticles brings the falling action. Consequently, as Pr grows, the thickness of the boundary layer shrinks. Table 5 shows a comparison of our results to the results presented by Jawad and Saeed [58]. In the absence of the nanoparticles and non-Newtonian paramaters, our results are identical to the Jawad and Saeed results. This comparison shows the accuracy and validity of our method.

Table 4: Numerical values of the Sherwood number $Re^{-1/2}Sh_x$.

N_t/N_b	0.2	0.4	0.6	0.8
0.1	0.407924	0.383741	0.375666	0.359017
0.2	0.457804	0.408919	0.392597	0.371618
0.3	0.5085591	0.434520	0.409789	0.384416
0.4	0.560222	0.460513	0.427223	0.410539
0.5	0.612637	0.486868	0.444879	0.423837

Table 5: Comparison of local Nusselt results in the absence of non-Newtonian and nanoparticle paramaters.

Re	Wang [64]	Present
0.7	0.4539	0.4539
2	0.9114	0.9114
7	1.8954	1.8954
20	3.3539	3.3539
70	6.4622	6.4622

5. Conclusion

The Oldroyd-B nanofluid model was presented across a stretched sheet for this investigation. The quantitative analysis of the impacts of thermophoresis parameter, elastic parameter, and Brownian motion on heat and flow transfer is studied here. Below are the key features of the study.

(1) For the mass fraction, temperature, and speed functions, β_1 and β_2 impacts have the opposite behavior. Such anomalies arise only because of the influence of β_1 and β_2 viscoelastic parameters

(2) Prandtl's actions are the same for both the temperature and mass fraction functions. As Pr is the link

among visual and dynamic viscosity, at greater Pr levels, the temperature profile remains under control

(3) Similar effects of N_b and N_t are seen on the temperature profile as both N_b and N_t increase the temperature

(4) For higher N_b values, regional Nusselt numbers are increasing in magnitude

(5) The local Sherwood number's size rises for high N_b numbers

(6) The electric field increasement increases the velocity and temperature profile, whereas the thermal radiation has reverse results

(7) The increases in magnetic field resist the flow, and so the velocity profile get decreases while it assists the temperature profile

(8) On increasing β and porosity parameters, the velocity distribution decreases

(9) Increase in the Pr thermal boundary-layer thickness and contraction profiles is noticed to decrease

(10) Increase in the Lewis number causes to decrease the profiles of velocity, temperature, and concentration

Abbreviations

Nomenclature

$\widetilde{B}$:	Magnetic field (NmA^{-1})
C:	Fluid concentration
c_p:	Specific heat $(J/\mathrm{kg}K)$
β:	Non-Newtonian paramter
$\tilde{E}$:	Electric field intensity (NC^{-1})
J_w:	Mass flux
$\alpha_1, \alpha_2, \beta_1, \beta_2, \beta_3$:	Material constants
A_1, A_2, A_3:	Kinematic tensors
k:	Thermal conductivity $(\mathrm{Wm}^{-1}\mathrm{K}^{-1})$
M:	Magnetic parameter
n_e:	Number density of electron
O:	Origin
P:	Fluid pressure (Pa)
Pr:	Prandtl number
Q_w:	Heat flux (Wm^{-2})
q_r:	Radioactive heat flux (J)
Re:	Viscosity parameter
S:	Cauchy stress tensor
t_e:	Flow time (s)
T:	Fluid temperature (K)
u, v, w:	Velocity components (ms^{-1})
x, y, z:	Coordinates
t:	Time.

Greek Letters

α:	Thermal diffusivity $(\mathrm{m}^2\mathrm{s}^{-1})$
$\widehat{\kappa}$:	Vertex viscosity (mPa)
μ:	Dynamic viscosity (mPa)
υ:	Kinematic coefficient of viscosity
ρ_f:	Base fluid density (kgm^{-3})
ρ_b:	Density of the particles (kgm^{-3}).

Data Availability

The data is available in the paper.

Conflicts of Interest

The authors declare that they have no conflicts of interest.

References

[1] M. C. Potter and D. C. Wiggert, *Schaum's outline of Fluid mechanics*, McGraw-Hill Education, 1996.

[2] F. M. White, *Viscose Fluid Flow*, McGraw-Hill, Inc, 1992.

[3] T. Altan, S. I. Oh, and G. Gegel, *Metal forming fundamentals and applications*, Metal Park: American Society of Metals, 1979.

[4] E. G. Fisher, *Extrusion of Plastics*, Wiley, New York, 1976.

[5] Z. Tadmor and I. Klein, *Engineering Principles of Plastic Ting Extrusion, Polymer Science and Engineering Series*, Van Nostrand Reinhold, New York, 1970.

[6] B. C. Sakiadis, "Boundary-layer behavior on continuous solid surfaces: III. The boundary layer on a continuous cylindrical surface," *Journal of the Taiwan Institute of Chemical Engineers*, vol. 7, no. 3, pp. 467–472, 1961.

[7] L. J. Crane, "Flow past a stretching plate," *Zeitschrift für Angewandte Mathematik und Physik*, vol. 21, no. 4, pp. 645–647, 1970.

[8] P. S. Gupta and A. S. Gupta, "Heat and mass transfer on a stretching sheet with suction or blowing," *The Canadian journal of chemical engineering*, vol. 55, no. 6, pp. 744–746, 1977.

[9] M. I. Char, "Heat transfer of a continuous, stretching surface with suction or blowing," *Journal of Mathematical Analysis and Applications*, vol. 135, no. 2, pp. 568–580, 1988.

[10] M. Turkyilmazoglu and I. Pop, "Exact analytical solutions for the flow and heat transfer near the stagnation point on a stretching/shrinking sheet in a Jeffrey fluid," *International Journal of Heat and Mass Transfer*, vol. 57, no. 1, pp. 82–88, 2013.

[11] S. Nadeem, S. Zaheer, and T. Fang, "Effects of thermal radiation on the boundary layer flow of a Jeffrey fluid over an exponentially stretching surface," *NumerAlgorith*, vol. 57, no. 2, article 187205, pp. 187–205, 2011.

[12] T. Hayat, M. Awais, S. Asghar, and A. A. Hendi, "Analytic solution for the magnetohydrodynamic rotating flow of Jeffrey fluid in a channel," *Journal of fluids engineering*, vol. 133, no. 6, article 0612017, 2011.

[13] M. Qasim, "Heat and mass transfer in a Jeffrey fluid over a stretching sheet with heat source/sink," *Alexandria Engineering Journal*, vol. 52, no. 4, pp. 571–575, 2013.

[14] S. Nadeem, R. U. Haq, and Z. H. Khan, "Numerical solution of non-Newtonian nanofluid flow over a stretching sheet," *Applied Nanoscience*, vol. 4, no. 5, pp. 625–631, 2014.

[15] T. Hayat, M. Awais, and S. Obaidat, "Three-dimensional flow of a Jeffery fluid over a linearly stretching sheet," *Communications in Nonlinear Science and Numerical Simulation*, vol. 17, no. 2, pp. 699–707, 2012.

[16] P. S. Narayana and D. H. Babu, "Numerical study of MHD heat and mass transfer of Jeffrey fluid over a stretching sheet with chemical reaction and thermal radiation," *Journal of the Taiwan Institute of Chemical Engineers*, vol. 59, p. 18, 2016.

[17] P. V. S. Narayana, "Effects of variable permeability and radiation absorption on magnetohydrodynamic (MHD) mixed convective flow in a vertical wavy channel with traveling thermal waves," *Propulsion and Power Research*, vol. 4, no. 3, pp. 150–160, 2015.

[18] P. S. Narayana, B. Venkateswarlu, and B. Devika, "Chemical reaction and heat source effects on MHD oscillatory flow in an irregular channel," *Ain Shams Engineering Journal*, vol. 7, no. 4, pp. 1079–1088, 2016.

[19] B. Venkateswarlu and P. V. Narayana, "MHD visco-elastic fluid flow over a continuously moving vertical surface with chemical reaction," *Walailak Journal of Science and Technology (WJST)*, vol. 12, no. 9, pp. 775–783, 2015.

[20] E. Magyari and B. Keller, "Heat and mass transfer in the boundary layers on an exponentially stretching continuous surface," *Journal of Physics D: Applied Physics*, vol. 32, no. 5, pp. 577–585, 1999.

[21] B. Bidin and R. Nazar, "Numerical solution of boundary layer flow over an exponentially stretching sheet with thermal radiation," *European journal of scientific research*, vol. 33, pp. 710–717, 2009.

[22] S. Mukhopadhyay and R. S. R. Gorla, "Effects of partial slip on boundary layer flow past a permeable exponential stretching sheet in presence of thermal radiation," *Heat and Mass Transfer*, vol. 48, no. 10, pp. 1773–1781, 2012.

[23] V. Singh and S. Agarwal, "MHD flow and heat transfer for Maxwell fluid over an exponentially stretching sheet with variable thermal conductivity in porous medium," *Thermal Science*, vol. 18, article 599615, suppl.2, pp. 599–615, 2014.

[24] F. K. Tsou, E. M. Sparrow, and R. J. Goldstein, "Flow and heat transfer in the boundary layer on a continuous moving surface," *International Journal of Heat and Mass Transfer*, vol. 10, no. 2, pp. 219–235, 1967.

[25] E. M. A. Elbashbeshy, "Heat Transfer over an Exponentially Stretching Continuous Surface with Suction," *Archives of Mechanics*, vol. 53, no. 6, pp. 643–651, 2001.

[26] S. U. S. Choi and J. A. Eastman, "Enhancing thermal conductivity of fluids with nanoparticles," in *Development and applications of non-Newtonian flows*, D. A. Siginer and H. P. Wang, Eds., p. 9910, ASME, 1995.

[27] L. Godson, B. Raja, D. M. Lal, and S. E. Wongwises, "Enhancement of heat transfer using nanofluids: an overview," *Renewable and sustainable energy*, vol. 14, no. 2, article 629641, pp. 629–641, 2010.

[28] S. M. Sebdani, M. Mahmoodi, and S. M. Hashemi, "Effect of nanofluid variable properties on mixed convection in a square cavity," vol. 52, pp. 112–126, 2012.

[29] W. A. Khan and I. Pop, "Boundary-layer flow of a nanofluid past a stretching sheet," *International Journal of Heat and Mass Transfer*, vol. 53, no. 11-12, pp. 2477–2483, 2010.

[30] W. A. Khan and A. Aziz, "Double-diffusive natural convective boundary layer flow in a porous medium saturated with a nanofluid over a vertical plate: Prescribed surface heat, solute and nanoparticle fluxes," *International Journal of Thermal Sciences*, vol. 50, no. 11, pp. 2154–2160, 2011.

[31] P. O. Olanrewaju, A. Olanrewaju, and A. O. Adesanya, "Boundary layer flow of nanofluids over a moving surface in a flowing fluid in the prescence of radiation," *International Journal of Applied Science and Technology*, vol. 2, 2012.

[32] J. Koo and C. Kleinstreuer, "Laminar nanofluid flow in microheat-sinks," *International Journal of Heat and Mass Transfer*, vol. 48, no. 13, article 26522661, pp. 2652–2661, 2005.

[33] S. K. Khan, M. S. Abel, and R. M. Sonth, "Visco-elastic MHD flow, heat and mass transfer over a porous stretching sheet with dissipation of energy and stress work," *Heat and Mass Transfer*, vol. 40, no. 1-2, pp. 47–57, 2003.

[34] M. Fiza, H. Ullah, and S. Islam, "Three dimensional MHD rotating flow of viscoelastic nanofluid in porous medium between two parallel plates," *Journal of Porous Media*, vol. 23, pp. 715–729, 2020.

[35] D. A. Nield and A. V. Kuznetsov, "The Cheng-Minkowycz problem for natural convective boundary-layer flow in a porous medium saturated by a nanofluid," *International Journal of Heat and Mass Transfer*, vol. 52, no. 25-26, pp. 5792–5795, 2009.

[36] M. A. A. Hamad and M. Ferdows, "Similarity solutions to viscous flow and heat transfer of nanofluid over nonlinearly stretching sheet," *Applied Mathematics and Mechanics*, vol. 33, no. 7, article 923930, pp. 923–930, 2012.

[37] M. A. Hamad and M. Ferdows, "Similarity solution of boundary layer stagnation-point flow towards a heated porous stretching sheet saturated with a nanofluid with heat absorption/generation and suction/blowing: a lie group analysis," *Communications in Nonlinear Science and Numerical Simulation*, vol. 17, no. 1, pp. 132–140, 2012.

[38] N. S. Akbar, S. Nadeem, T. Hayat, and A. A. Hendi, "Peristaltic flow of a nanofluid in a non-uniform tube," *Heat and Mass Transfer*, vol. 48, no. 3, pp. 451–459, 2012.

[39] N. S. Akbar, S. Nadeem, T. Hayat, and A. A. Hendi, "Peristaltic flow of a nanofluid with slip effects," *Meccanica*, vol. 47, no. 5, pp. 1283–1294, 2012.

[40] A. N. Akbar and S. Nadeem, "Peristaltic flow of a Phan-Thien-Tanner nanofluid in a diverging tube," *Heat Transfer Asian Research*, vol. 41, no. 1, pp. 10–22, 2012.

[41] R. Ellahi, T. Hayat, F. M. Mahomed, and A. Zeeshan, "Exact solutions of flows of an Oldroyd 8-constant fluid with nonlinear slip conditions," vol. 65, no. 12, pp. 1081–1086, 2010.

[42] R. Ellahi, M. Raza, and K. Vafai, "Series solutions of non-Newtonian nanofluids with Reynolds' model and Vogel's model by means of the homotopy analysis method," *Mathematical and Computer Modelling*, vol. 55, no. 7-8, pp. 1876–1891, 2012.

[43] A. Zeeshan, R. Ellahi, A. M. Siddiqui, and H. U. Rahman, "An investigation of porosity and magnetohydrodynamic flow of non-Newtonian nanofluid in coaxial cylinders," *International Journal of Physical Sciences*, vol. 7, no. 9, pp. 1353–1361, 2012.

[44] O. D. Makinde, W. A. Khan, and Z. H. Khan, "Buoyancy effects on MHD stagnation point flow and heat transfer of a nanofluid past a convectively heated stretching/shrinking sheet," *International Journal of Heat and Mass Transfer*, vol. 62, pp. 526–533, 2013.

[45] H. Ullah, I. Khan, M. Fiza et al., "MHD boundary layer over a stretching sheet: a new stochastic method," *Mathematical*

Problems in Engineering, vol. 2021, Article ID 9924593, 26 pages, 2021.

[46] I. Khan, H. Ullah, H. AlSalman et al., "Falkner Skan equatin with heat transfer: A new stochastic numerical approach," *Mathematical Problems in Engineering*, vol. 2021, Article ID 3921481, 17 pages, 2021.

[47] H. Bilal, H. Ullah, S. Islam et al., "A Levenberg-Marquardt backpropagation method for unsteady squeezing flow of heat and mass transfer behaviour between parallel plates," *Advances in Mechanical Engineering*, vol. 13, no. 10, 2021.

[48] R. A. Khan, H. Ullah, M. A. Raja, M. A. Khan, S. Islam, and M. Shoaib, "Heat transfer between two porous parallel plates of steady nano fludis with Brownian and thermophoretic effects: a new stochastic numerical approach," *International Communications in Heat and Mass Transfer*, vol. 126, article 105436, 2021.

[49] H. Ullah, I. Khan, H. AlSalman et al., "Levenberg–Marquardt backpropagation for numerical treatment of micropolar flow in a porous channel with mass injection," *Complexity*, vol. 2021, Article ID 5337589, 12 pages, 2021.

[50] H. Ullah, M. Shoaib, R. A. Khan, M. A. Z. Raja, and S. Nisar, "Heat transfer impacts on Maxwell nanofluid flow over a vertical moving surface with MHD using stochastic numerical technique via artificial neural networks," *Coatings*, vol. 11, p. 1483, 2021.

[51] H. Ullah, R. A. Khan, M. Fiza, S. Islam, and S. M. Al-Mekhlafi, "Comparative evaluation of the optimal auxiliary function method and numerical method to explore the heat transfer between two parallel porous plates of steady nanofluids with Brownian and thermophoretic influences," *Mathematical Problems in Engineering*, vol. 2022, Article ID 7975101, 16 pages, 2022.

[52] H. Ullah, H. Khan, M. Fiza, K. Ullah, S. Islam, and S. M. al-Mekhlafi, "Comparative analysis of the effect of Joule heating and slip velocity on unsteady squeezing nanofluid flow," *Mathematical Problems in Engineering*, vol. 2022, Article ID 8452862, 10 pages, 2022.

[53] H. Ullah, M. Arif, M. Fiza, M. Ayaz, K. Ullah, and S. Makhlafi, "Analytical and numerical analysis of the squeezed unsteady MHD nanofluid flow in the presence of thermal radiation," *Journal of Nanomaterials*, vol. 2022, Article ID 1668206, 14 pages, 2022.

[54] A. Tassaddiq, S. Khan, M. Bilal et al., "Heat and mass transfer together with hybrid nanofluid flow over a rotating disk," *AIP Advances*, vol. 10, no. 5, article 055317, 2020.

[55] W. Khan, M. Idress, T. Gul, M. A. Khan, and E. Bonyah, "Three non-Newtonian fluids flow considering thin film over an unsteady stretching surface with variable fluid properties," *Advances in Mechanical Engineering*, vol. 10, no. 10, 2018.

[56] T. Gul, S. Islam, R. A. Shah, A. Khalid, I. Khan, and S. Shafie, "Unsteady MHD thin film flow of an Oldroyd-B fluid over an oscillating inclined belt," *PloS one*, vol. 10, no. 7, article e0126698, 2015.

[57] M. Bilal, A. Saeed, T. Gul, I. Ali, W. Kumam, and P. Kumam, "Numerical approximation of microorganisms hybrid nanofluid flow induced by a wavy fluctuating spinning disc," *Coatings*, vol. 11, no. 9, p. 1032, 2021.

[58] M. Jawad, A. Saeed, and T. Gul, "Entropy generation for MHD Maxwell nanofluid flow past a porous and stretching surface with Dufour and Soret effects," *Brazilian Journal of Physics*, vol. 51, no. 3, pp. 469–480, 2021.

[59] T. Gul, R. S. Gul, W. Noman et al., "CNTs-nanofluid flow in a rotating system between the gap of a disk and cone," *Physica Scripta*, vol. 95, no. 12, article 125202, 2020.

[60] K. J. Bathe, *Finite Element Procedures*, Prentice-Hall, New Jersey, USA, 1996.

[61] J. N. Reddy, *An Introduction to the Finite Element Method*, McGraw-Hill, New York, 1985.

[62] J. J. Connor and C. A. Brebbia, *Finite Element Techniques for Fluid Flow*, Butterworths, London, 1976.

[63] S. Nadeem, R. Haq, N. S. Akbar, C. Lee, and Z. H. Khan, "Numerical Study of Boundary layer flow and heat transfer of Oldroyd-B nanofluid towards a stretching sheet," *Plos One*, vol. 8, no. 8, article e69811, 2013.

[64] C. Y. Wang, "Free convection on a vertical stretching surface," *Journal of Applied Mathematics and Mechanics*, vol. 69, no. 11, pp. 418–420, 1989.